Langmuir
Article
pubs.acs.org/Langmuir

Do Electrospun Polymer Fibers Stick?

Qiang Shi,[†,⊥] Kai-Tak Wan,[§] Shing-Chung Wong,*[,†] Pei Chen,[†] and Todd A. Blackledge[‡]

[†]*Department of Mechanical Engineering, and* [‡]*Department of Biology, The University of Akron, Akron, Ohio 44325-3903, and* [§]*Department of Mechanical and Industrial Engineering, Northeastern University, Boston, Massachusetts 02115.* [⊥] *Present address: State Key Laboratory of Polymer Physics and Chemistry, Changchun Institute of Applied Chemistry, Chinese Academy of Sciences, Changchun 130022, China.*

Received March 28, 2010. Revised Manuscript Received July 23, 2010

Adhesion between electrospun polycaprolactone (PCL) fibers was directly measured in a cross-cylinder geometry using a nanoforce tensile tester. The surface roughness of fibers was determined by an atomic force microscope (AFM), and the structural factors were characterized by differential scanning calorimeter (DSC) and wide-angle X-ray diffraction (WAXD). "Pull-off" force was found to be in the order of 10^{-6} N, and the adhesion energy was 190 ± 7 mJ/m^2. Adhesion increases with decreasing fiber radius. The experimental data are analyzed by the classical Johnson−Kendall−Roberts (JKR) contact mechanics model. The study provides fruitful insights into future development of bio-inspired adhesives and devices.

1. Introduction

Hierarchical structures as inspired from nature, such as the fibrils on insects, induce strong molecular forces as a result of van der Waals (vdW) interactions. The subsequent extraordinarily strong adhesion enables these insects to support their body weight and large loads.[1−4] This phenomenon motivated materials scientists and engineers to fabricate artificial fibrillar adhesives using materials ranging from soft polymers[4−8] to stiff carbon nanotubes.[3,9,10] To leapfrog, it is critical to understand the mechanics and mechanisms of fiber−fiber interactions in terms of molecular parameters.

Adhesion between fiber and substrate was extensively studied in recent years.[2,6,11] The Johnson−Kendal−Robert (JKR)[12,13] and Derjaguin−Muller−Toporov (DMT)[14] models are particularly useful in modeling contact mechanics of adhesion−detachment. Despite studies in the deformation, orientation, geometry, and size of fiber showing substantial effects on the fiber−substrate adhesion,[2,11] little is known about fiber−fiber adhesion, mainly due to experimental difficulties in handling and aligning micro- and nanofibers and choosing the appropriate characterization instrument.

We utilize an electrospinning technique to produce well-controlled submicrometer fibers with fiber radius ranging from 300 to 900 nm on average.[15−17] The strong electrostatic force stretches the polymer jet to simultaneously reduce the cross-sectional area and lengthen the fiber to an aspect ratio as high as 10^6. Fiber alignment can be achieved by collecting the fibers on a rotating, grounded disk[18−21] or across two parallel, conductive strips.[22] The mechanical properties[20−23] are shown to depend on drawing[20,21] and molecular characteristics of the fibers. Measurements of adhesion properties of electrospun fibers and bundles are herein performed for the first time using a nanoforce tensile tester with a force/displacement resolutions of 50 nN/10 nm, respectively. The same instrument has been used to examine the adhesion properties between spider silk fibers, and the results are reported elsewhere.[24,25]

In this paper, we report the "pull-off" force and interfacial adhesion between two electrospun fibers in a novel cross-cylinder configuration similar to the celebrated surface force apparatus (SFA). The dependence of adhesion upon size effect (fiber diameter) and surface roughness is investigated and will be discussed in terms of the JKR model and molecular factors.

2. Experimental Section

2.1. Materials. Biodegradable polymer, polycaprolactone (PCL) (M_n = 80 000), was purchased from Sigma-Aldrich (CAS = 24980-41-4) and dried under vacuum at 40 °C for 36−48 h before use. *N,N*-Dimethylformamide (DMF) and dichloromethane (DCM) at reagent grade were obtained from Acros and BMD Chemicals Inc., respectively.

*Corresponding author: Ph +1-330-972-8275; Fax +1-330-972-6027; e-mail swong@uakron.edu.

(1) Maderson, P. F. A. *Nature* **1964**, *203*, 780–781.
(2) Autumn, K.; Liang, Y. A.; Hsieh, S. T.; Zesch, W.; Chan, W.-P.; Kenny, W. T.; Fearing, R.; Full, R. J. *Nature* **2000**, *405*, 681–685.
(3) Autumn, K.; Sitti, M.; Liang, Y. A.; Peattie, A. M.; Hansen, W. R.; et al. *Proc. Natl. Acad. Sci. U.S.A.* **2002**, *99*, 12252–12256.
(4) Geim, A. K.; Dubonos, S. V.; Grigorieva, I. V.; Novoselov, K. S.; Zhukov, A. A.; Shapoval, S. Y. *Nature Mater.* **2003**, *2*, 461–463.
(5) Kim, S.; Sitti, M. *Appl. Phys. Lett.* **2006**, *89*, 26911–26913.
(6) Gorb, S.; Varenberg, M.; Peressadko, A.; Tuma, J. *J. R. Soc. Interface* **2007**, *4*, 271–275.
(7) Kim, S.; Cheung, E.; Sitti, M. *Langmuir* **2009**, *25*, 7196–7199.
(8) Lee, J.; Bush, B.; Maboudian, R.; Fearing, R. S. *Langmuir* **2009**, *25*, 12449–12453.
(9) Lee, H.; Lee, B. P.; Messersmith, P. B. *Nature* **2007**, *448*, 338–342.
(10) Fischer, K. E.; Aleman, B. J.; Tao, S. L.; Daniels, R. H.; Li, E. M.; Bonger, M. D.; Ganesh Nagaraj, G.; Singh, P.; Zettl, A.; Desai, T. A. *Nano Lett.* **2009**, *9*, 716–720.
(11) Gao, H.; Yao, H. *Proc. Natl. Acad. Sci. U.S.A.* **2004**, *101*, 7851–7856.
(12) Johnson, K. L.; Kendall, K.; Roverts, A. D. *Proc. R. Soc. London A* **1971**, *324*, 301–303.
(13) Maugis, D. *J. Colloid Interface Sci.* **1992**, *150*, 243–269.
(14) Derjaguin, B. V.; Muller, V. M.; Toporov, Y. P. *J. Colloid Interface Sci.* **1975**, *53*, 314–326.
(15) Dzenis, Y. *Science* **2004**, *304*, 1917–1919.
(16) Reneker, D. H.; Yarin, A. L.; Zussman, E.; Xu, H. *Adv. Appl. Mech.* **2007**, *41*, 43–195.
(17) Reneker, D. H.; Yarin, A. L. *Polymer* **2008**, *49*, 2387–2425.
(18) Theron, A.; Zussman, E.; Yarin, A. L. *Nanotechnology* **2001**, *12*, 384–390.
(19) Zussman, E.; Theron, A.; Yarin, A. L. *Appl. Phys. Lett.* **2003**, *82*, 973–975.
(20) Zussman, E.; Rittel, D.; Yarin, A. L. *Appl. Phys. Lett.* **2003**, *82*, 3958–3960.
(21) Zussman, E.; Burman, M.; Yarin, A. L.; Khalfin, R.; Cohen, Y. *J. Polym. Sci., Part B: Polym. Phys.* **2006**, *44*, 1482–1489.
(22) Wong, S.-C.; Baji, A.; Leng, S. *Polymer* **2003**, *49*, 4713–4722.
(23) Tan, E. P. S.; Ng, S. Y.; Lim, C. T. *Biomaterials* **2005**, *26*, 1453–1456.
(24) Blackledge, T. A.; Cardullo, R. A.; Hayashi, C. Y. *Invertebr. Biol.* **2005**, *124*, 165–173.
(25) Sahni, V.; Blackledge, T. A.; Dhinojwala, A. *Nature Commun.* **2010**, *1*(19), 1–4.

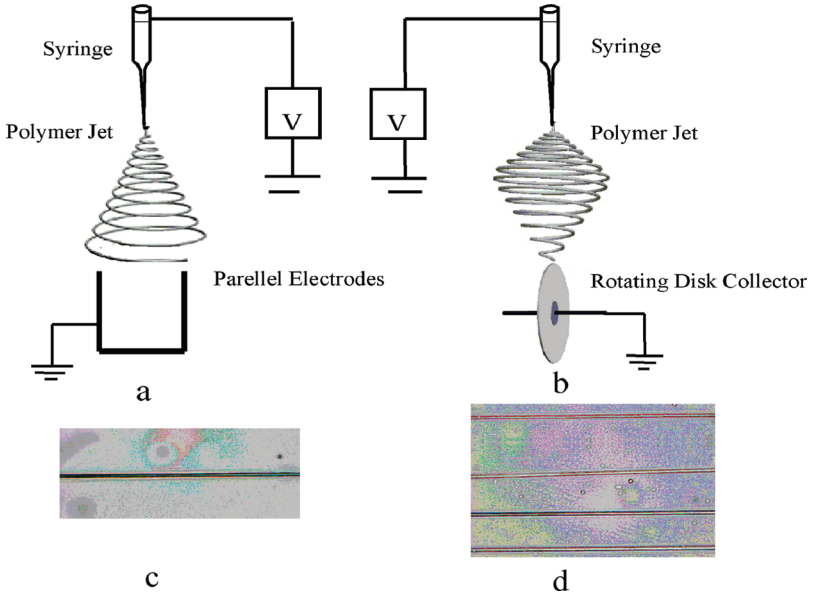

Figure 1. Schematic of method used to collect single and aligned fibers. (a) A single fiber is collected by parallel electrodes for tensile and adhesion tests. (b) Aligned fibers are collected by the rotational disk for DSC, PLM, and WAXD tests. (c) PLM micrograph of a single fiber; the magnification is 1000×. (d) PLM micrograph of aligned fibers that are collected for 20 s; the magnification is 1000×.

2.2. Samples Preparation. Polymer fibers are fabricated for dry adhesion studies, tensile tests, and fiber structural characterization, using the electrospinning technique (shown in Figure 1).[18,20,22] The fibers are electrospun from two solutions with 12 and 14 wt % PCL. The polymer is first dissolved in a solvent mixture of DMF and DCM with a 1:1 weight ratio. Electrospinning is conducted at 22 °C, relative humidity at 43%, solution feed rate at 0.5 mL/h, and applied voltage at 10−11 kV. The fibers are collected by either (a) two parallel electrodes (Figure 1a) or (b) a collector disk.

Single fibers made by the parallel electrodes are used for tensile tests.[22] Specimens for adhesion measurement are prepared by first collecting as-spun fibers on a primary collector comprising two parallel electrodes, followed by transferring single fibers onto a secondary collector.[23] The fiber collection is carried out for a short duration for a few aligned single fibers on the parallel electrodes. The secondary collector is a cardboard frame with a 15 mm gap between two parallel strips. A single fiber is transferred to cardboard frame, fixed by adhesive tapes, and suspended as a freestanding wire. Directional fiber bundle is obtained from a rotational disk collector at a tangential velocity from 20 to 35 m/s.[18,20] The alignment of fibers is measured relative to one another and is characterized by a standard deviation of 2.4°. The fiber bundle was used for DSC and X-ray measurements. Figures 1c,d show the optical micrographs of typical fibers obtained by polarized light microscopy (Leica DMLB). Cross-sectional diameter is measured at six different locations using the software NIH Image 1.63 (Figures 1c,d).[24]

2.3. Adhesion Measurements. Figure 2 shows the schematic of the adhesion measurement. A single freestanding fiber is taped to the two prongs of a cardboard mount that are $2l_0 = 15$ mm apart (Figure 2a). The cardboard is then sectioned by a pair of scissors leaving two selected fibers for the adhesion test. Two cardboard holders with the fibers are mounted onto the moveable crosshead and fixed load cell of an MTS Nano Bionix system. The two freestanding fibers are arranged orthogonal to each other at the midpoint in a cross-cylinder configuration (Figure 2b). The crosshead is then moved to an approach distance of 1 mm such that the fibers are pressed against each other leading to an adhesive contact at an ambient relative humidity of ~20%. The compression lasts for roughly 20 min to ensure proper adhesion. Though slightly stronger adhesion is observed with increasing fiber−fiber contact time up to 1 h, an optimal 20 min contact time is set for the current study. The contact circle has a diameter of $2a$ (Figure 2c). The crosshead is then returned to the original position such that the two fibers resume stress free and horizontal geometry. A tensile load is then applied to pull on the fibers with the crosshead moving at 1.0 mm s^{-1}. The applied load, F, and vertical displacement, u, are simultaneously monitored, while a video camera records the sample deformation *in situ*. Measurements are repeated at least 10 times for a single pair of fibers to ensure reproducibility.

2.4. AFM Measurements. The AFM used is a SPI3800N systems equipped with a cantilever of bending spring constant 40 N/m and a resonance frequency of 190 kHz (SEIKO, Inc.). The fiber surface is characterized by the standard noncontact mode scanning at 0.5 Hz from the largest area (100 × 100 μm^2) to smallest area of 5 × 5 μm^2. Data are analyzed using the SPI3800N probe station software (Seiko, Inc.). All images are processed using procedures for "plan-fit" and "flatten". The roughness is determined by the software based on a line profile along the electrospun fiber axis at different positions. At least 10 lines are drawn for different positions used. An average roughness (R_a) of the fiber surface is calculated with the methods used by Watanabe and co-workers.[26]

2.5. Differential Scanning Calorimetry (DSC). The melt-processed PCL fiber is further characterized by differential scanning calorimetry using a Perkin-Elmer DSC-7. The degree of crystallinity (X_c) of PCL fibers is found by $\Delta H_m/\Delta H_{m0}$, where ΔH_m is the enthalpy of melting and ΔH_{m0} the enthalpy of melting of fully crystalline PCL (139.5 J/g).[27]

2.6. Polarized Light Microscopy (PLM). The electrospun fibers are observed between crossed polarizers in a Leica DMLP optical microscope equipped with a camera system (Leica MPS30). In order to enhance contrast and determine the sign of the birefringence pattern, a λ wave plate is inserted between the polarizers.

2.7. Wide-Angle X-ray Diffraction (WAXD). WAXD is conducted using a D8-GADDS diffractometery (Bruker) with a 2D detector. The measurements are carried out at 40 kV and 20 mA, Cu Kα radiation. X-ray beam is directed perpendicular to the fiber bundle axis. The distance between the detector and the sample for WAXD is 147.8 mm. The orientation factor of the

(26) Miwa, M.; Nakajima, A.; Fujishima, A.; Hashimoto, K.; Watanabe, T. *Langmuir* **2000**, *16*, 5754–5760.
(27) Lee, K. H.; Kim, H. Y.; Khil, M. S.; Ra, Y. M.; Lee, D. R. *Polymer* **2003**, *44*, 1287–1294.

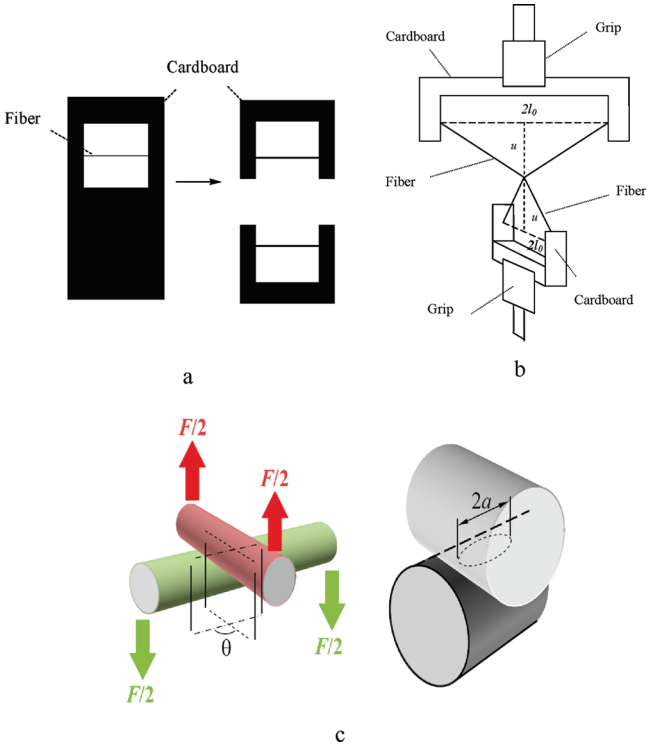

Figure 2. Schematic of the dry adhesion test. Single freestanding fiber with original length of $2L_0$ is taped to the two prongs of a cardboard, and the single fibers with the same radius are used for the dry adhesion test (a). The cardboards are cut into U shapes and mounted on the nanoforce tensile tester with a load resolution of 50 nN and extension resolution of 35 nm (b). Two fibers are arranged in the cross-cylinder geometry, and the contact circle has a diameter of $2a$ (c). Vertical compressive load deforms the two fibers into V- and inverted V-shapes, and the force (F) and displacement (u) are simultaneously recorded.

crystallites and the order parameter of amorphous phase are determined with the same method reported by Zussman and co-workers.[28]

3. Results and Discussion

3.1. Mechanical Response of External Load. Figure 3 shows typical mechanical responses and applied load as a function of vertical displacement, $F(u)$, for a range of fiber radii, R_0. Three distinct regions are identified: (I) Elastic stretching of fibers where no delamination takes place. Linear elasticity requires $F = E[\pi R_0^2 u(l - l_0)/l_0 l]$, where E is the elastic modulus, l the instantaneous half-length, and the subscript 0 the undeformed quantities. (II) A plateau exhibiting virtually a constant load where gradual delamination occurs. (III) A precipitous drop when the applied load reaches a critical threshold, F^*. At this "pull-off" point, the adhering fibers spontaneously separate from each other and F drops abruptly (see Supporting Information, video of adhesion test). No slippage is observed at the fiber−cardboard interface. The "pull-off" load, or dry adhesive force, lies in the range of 10^{-6} N, consistent with typical van der Waals interactions.[2,3,29] Figure 3 shows a thicker fiber leads to an increasing "pull-off" force.

3.2. Size-Dependent Adhesion. Adhesion in the cross-cylinder configuration can be quantified by the classical Johnson−Kendall−Roberts (JKR)[12,13,30] and Derjaguin−Muller−Toporov

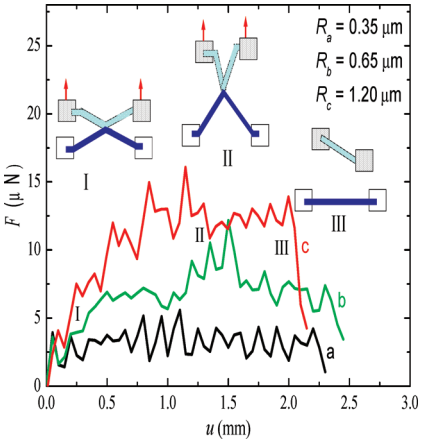

Figure 3. Applied external load F measured as a function of crosshead displacement u for PCL fibers of three different radii. The inset depicts the crossed fibers at initial stage, V- and inverted V-shaped deformation, and "pull-off", corresponding to the linear elastic deformation zone, load plateau, and spontaneous loss of adhesion contact exhibited in $F-u$ plot. Dry adhesion increases with an increasing fiber radius.

(DMT)[14] models for two identical adhering solid spheres or two equal crossed cylinders with a radius, R, elastic modulus, E, and Poisson's ratio, ν. The JKR limit corresponds to the presence of a short-range intersurface attraction and soft adhering solids, while the DMT limit is valid for long-range attraction and hard solids. The continuous transition from JKR to DMT is governed by the Tabor parameter[13,14,30]

$$\mu_T = \left(\frac{R'W^2}{Z_0^3}\right)^{1/3}\left(\frac{E}{2(1-\nu^2)}\right)^{-2/3} \quad (1)$$

where Z_0 is the range of the intersurface attraction, $R' = R/2$, W is the adhesion energy or work of adhesion, and $K = 2E/3(1-\nu^2)$ is the combined elastic modulus of two fibers. Maugis[13] derived an equivalent JKR−DMT transition parameter given by $\mu_M = 1.1570\mu_T$. The JKR limit possesses a large μ_T (>2) and DMT a small μ_T (<0.5).

For PCL fibers, the Young's modulus of fiber is determined by a tensile test, and the typical vdW force range is $Z_0 \approx 1$ nm. Reported values of $W = 53$ mJ/m^2 and $\nu = 0.47$ suggest a large μ_T and thus the JKR limit.[31,32] When the applied tensile load reaches the "pull-off" threshold

$$F^* = (3/2)\pi RW \quad (2)$$

the adhering fibers detach from each other. Figure 4 shows measured F^* as a monotonic increasing function of R in a log−log plot. Curve fit shows a slope of 1, as expected. The adhesion energy is deduced from the vertical intercept to be $W = 190 \pm 7$ mJ/m^2, independent of R. Table 1 shows an increasing E with decreasing R, and μ_T falls in the range of $5.54 < \mu < 9.98$, verifying our assumption of JKR limit.[12,14] As a comparison, the adhesion energy of PCL membranes was previously estimated based on a symmetrical contact between two identical films,[12] where the surface energy was quoted to be $W = 26.5$ mJ/m^2 by contact angle measurements.[31] The adhesion energy of PCL fibers in our measurement is significantly higher than that of PCL films at

(28) Arinstein, A.; Burman, M.; Gendelman, O.; Zussman, E. *Nature Nanotechnol.* **2007**, *2*, 59–62.
(29) Kendall, K. *Science* **1994**, *263*, 1720–1725.
(30) Shi, X.; Polycarpou, A. A. *J. Colloid Interface Sci.* **2005**, *281*, 449–457.
(31) Erbil, H. Y.; Yasuar, B.; Suzer, S.; Baysal, B. M. *Langmuir* **1997**, *13*, 5484–5493.
(32) Chen, B.; Evans, J. R. G. *Macromolecules* **2006**, *39*, 747–754.

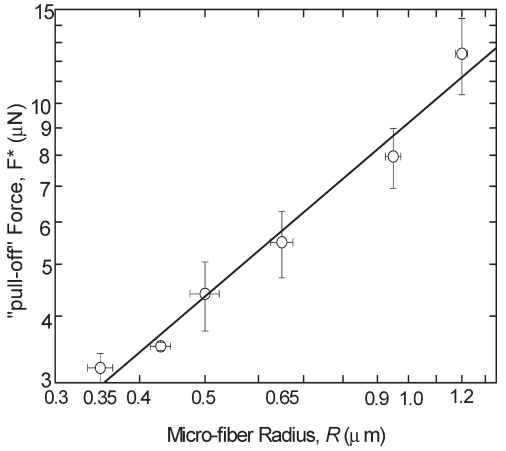

Figure 4. Measured "pull-off" force as a function of fiber radius. Data are fitted to a linear relationship according to the JKR theory.

Table 1. Tabor Parameter and the Parameters Used

fiber radius R (μm)	adhesion energy W (mJ/m^2)	Young's modulus E (MPa)	Poisson's ratio[a] ν	Tabor parameter[b] μ_T
0.25	190	300	0.47	5.54
0.44	190	297	0.47	6.02
0.55	190	292	0.47	6.56
0.65	190	286	0.47	7.04
0.90	190	280	0.47	7.95
1.20	190	230	0.47	9.98

[a] PCL pellets.[32] [b] Range of intersurface forces or equilibrium separation, $Z_0 \approx 1$ nm.

53 mJ/m^2, hydrocarbon rubber spheres films at 71 mJ/m^2, and polydimethylsiloxane (PDMS) rubber spheres at 43.6 mJ/m^2,[29] suggesting that polymer fibers possess higher adhesion than that derived from films or bulk materials. The high adhesion energy of PCL fibers is essentially dominated by multiscale surface effect.[33] It is plausible that interdiffusion of polymer chains takes place at the fiber interfaces (with the amorphous phase) due to the low glass transition temperature (−60 °C) and low melting point (60 °C) of PCL fibers. The latter may also raise adhesion energy and μ_T, further justifying the JKR limit assumption.[13,30,34]

3.3. Size-Dependent Adhesive Strength. The adhesive strength is defined herein as the adhesive force per unit contact area at "pull-off", F^*/S, with $S = \pi(a^*)^2$ and a^* the "pull-off" radius. The JKR model requires

$$a^* = (9WR^2/4E)^{1/3} \quad (3)$$

Based on eqs 2 and 3, the adhesive strength is

$$F^*/S = (2/3WE^2)^{1/3}R^{-1/3} \quad (4)$$

Figure 5 shows F^*/S as a function of R. The linear log−log curve fit yields a slope of −0.42, slightly lower than the expected value of −0.33, possibly a consequence of the size-dependent elastic modulus. It is interesting to note that the value of F^*/S increases with decreasing fiber radius, from 20 kN/cm^2 for $R = 1.2$ μm to 30 kN/cm^2 for $R = 0.35$ μm. This is consistent with the natural adhesion, e.g., feet of flies, beetles, spiders, and geckos, where the density of adhesive hairs increases dramatically with body weight.[35] A simple geometry argument gives the total adhesive strength, $F^*/S = (3/2)\pi RWn$, where n is the number density with n = cross-sectional area of fiber/foot area. As an illustration, we can compare the adhesion of two fibers with one cross-sectional radius doubled that of the other ($R_1 = R = 2R_2$) but of same adhesion energy. For fiber 1, only one fiber can fit into an area of R^2, and therefore the total adhesion force is $F_1 = (3/2)\pi RW$. For fiber 2, four fibers can fit into an area of R^2, and the total adhesion force is $F_2 = 3\pi RW = 2F_1$. A higher fiber density is therefore necessary to support a larger body weight.

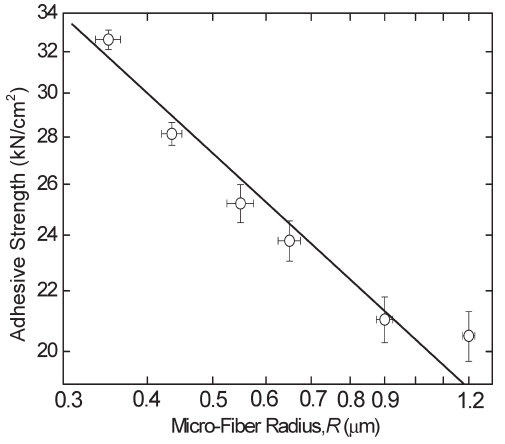

Figure 5. Adhesive strength as a function of fiber radius. The adhesion strength increases with decreasing fiber radius.

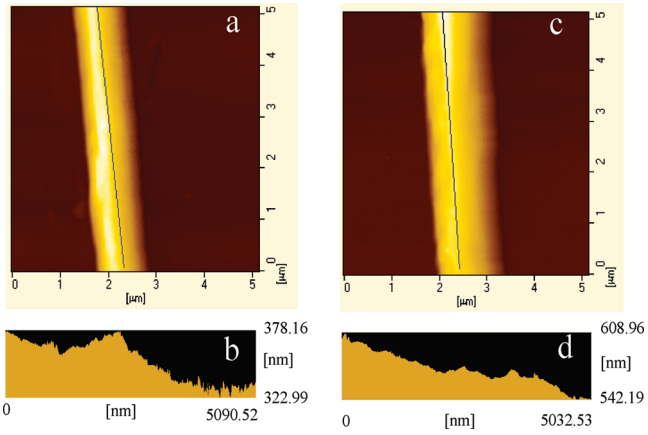

Figure 6. AFM topographic images and line profiles of electrospun fibers: (a) electrospun fiber with a radius of 0.55 μm; (b) a line profile of the surface along the fiber axis with the radius of 0.55 μm; (c) electrospun fiber with a radius of 0.65 μm; (d) a line profile of the surface along the fiber axis with the radius of 0.65 μm. Surface roughness is determined by the line profile along the fiber axis. The average roughness for 0.55 and 0.65 μm fibers are 3.3 and 4.2 nm, respectively. The roughness is broadly insignificant in comparison with the size of the electrospun fibers.

3.4. Effect of Roughness on Adhesion. Figure 6 shows the AFM images of electrospun fibers with $R = 0.55$ and 0.65 μm. The fiber roughness can be characterized by AFM by scanning along the fiber axis. Figure 7 shows dependence of average fiber roughness (R_a) upon fiber radius. Fiber roughness in the range of 2−7 nm is 2 orders of magnitude smaller than the fiber diameter. The smooth fiber surface is not expected to influence our adhesion measurements.

3.5. Effect of Molecular Orientation. By rotating the fibers under cross-polarized light, birefringence is clearly observed in

(33) Cuenot, S.; Frétigny, C.; Demoustier-Champagne, S.; Nysten, B. *Phys. Rev. B* **2004**, *69*, 165410.
(34) Schach, R.; Tran, Y.; Menelle, A.; Creton, C. *Macromolecules* **2007**, *40*, 6325–6332.
(35) Gorb, S.; Sinha, M.; Peressadko, A.; Daltorio, K. A.; Quinn, R. D. *Bioinspiration Biomimetics* **2007**, *2*, S117–S125.

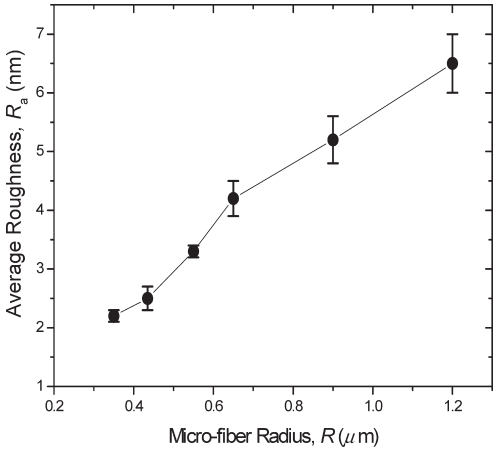

Figure 7. Average surface roughness of fiber surface as a function of fiber radius. The surface roughness (R_a) lies in the range of 2−7 nm, indicating the fiber is smooth.

our samples, suggesting the presence of chain orientation and/or crystallization.[16,20] Figure 8 shows the WAXD pattern for (a) PCL nonwoven mats and three electrospun fibers with average fiber radii of (b) 0.55, (c) 0.41, and (d) 0.35 μm. There are two strong diffraction arcs (or rings) at Bragg angles 2θ = 21.6° and 24° observed for all the samples tested. The equatorial peak at 21.6° is attributed to the diffraction of the (110) lattice plane and the peak at 24° attributed to the (200) lattice plane, which is usually seen in orthorhombic semicrystalline PCL.[36] The arc width of the strongest equatorial reflection provides a strong indication of the degree of orientation within the samples. The rings observed in the WAXD data for nonwoven mats are indicative of the random orientation of fibers. In contrast, the aligned fibers show a distinctive molecular orientation, as detected by the discrete reflections in Figures 8b−d. Most importantly, the larger fibers have less a degree of orientation compared to the smaller ones.

Figure 9 demonstrates the degree of crystallinity (%), orientation degree of crystallite, and order parameter of macromolecular orientation in the amorphous regions. They all increase with decreasing fiber radius, and the orientation degree of crystallite increases from 79.5% (R = 1.20 μm) to 93.2% (R = 0.35 μm). Clearly, molecular orientation is enhanced by electrospinning and reducing the fiber diameter. The crystallinity of PCL fibers as measured in our study (53.1%) is lower than 66.28%, which is the one reported by Yarin and co-workers, and it is almost the same as the PCL pellets.[37] The difference can be caused by the difference in average fiber sizes being examined (700 nm in this study vs 540 nm[37]). Some reports of lower degree of crystallinity in electrospun fibers in comparison to the bulk materials like pellets are noted.[38−40] The lower crystallinity in electrospun fibers vs bulk materials is attributed to rapid solidification of stretched chains at high elongational flows at the later stage of spinning, and the stretched chains do not have enough time to organize themselves into suitable crystal registration before they are solidified.[38−40] The orientation of crystals in the electrospun fiber

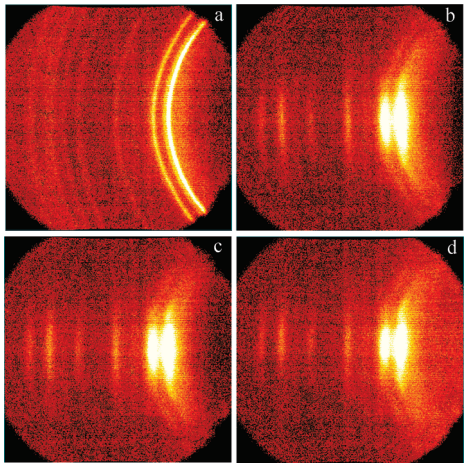

Figure 8. Wide-angle X-ray diffraction (WAXD) pattern of electrospun fibers: (a) PCL nonwoven mats; (b) aligned fiber bundle with an average fiber radius of 0.55 μm; (c) aligned fiber bundle with an average fiber radius of 0.41 μm; (d) aligned fiber bundle with an average fiber radius of 0.35 μm.

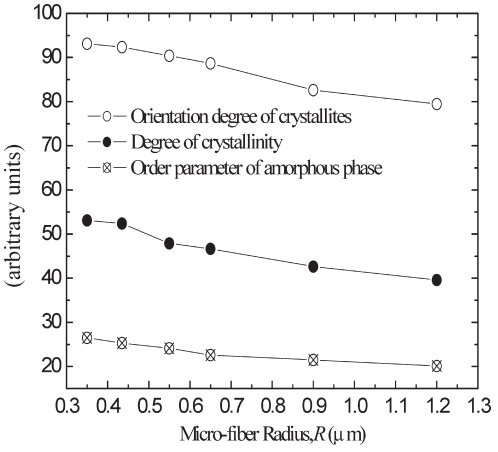

Figure 9. Crystallinity (%), crystallite orientation (%), and order parameter of macromolecular orientation in the amorphous phase as a function of fiber radius of aligned fibers. The degree of crystallinity, crystallites orientation, and order parameter of amorphous phase increase gradually as the fiber radius decreases. The degree of crystallinity increases from 39.6% (1.2 μm) to 53.1% (0.35 μm), the orientation degree of crystallite increases from 79.5% (1.2 μm) to 93.2% (0.35 μm), and the order parameter of macromolecular orientation in the amorphous part increases from 20.3% (1.2 μm) to 26.5% (0.35 μm).

will be however substantially higher than the bulk because the electrified jet of polymer solution experiences strong extensional flow during the electrospinning, and the polymer chains have a higher tendency to be stretched along the jet axis.[15,16,20] In addition, the crystallization of polymer chains is promoted by the whipping motion of the jet before the fiber reaches the collector. The order parameter of macromolecular orientation in the amorphous part increases in smaller fibers, from 20.3% (R = 1.20 μm) to 26.5% (R = 0.35 μm).

Apparently, enhanced molecular orientation leads to better mechanical properties[22] and potentially better adhesion. A qualitative reasoning can be given as follows: the high degree of crystallinity and molecular orientation align the "temporary dipoles" within the fiber, resulting in uneven charges on the fiber surface. These vdW forces are transient because of the constantly changing electron distributions but are continuously switching on

(36) Bittiger, H.; Marchessault, R. H.; Niegisch, W. D. *Acta Crystallogr., Sect. B* **1970**, *26*, 1923–1927.
(37) Srikar, R.; Gambaryan-Roisman, T.; Steffes, C.; Stephan, P.; Tropea, C.; Yarin, A. L. *Int. J. Heat Mass Transfer* **2009**, *52*, 5814–5826.
(38) Liu, W.; Wu, Z.; Reneker, D. H. *Polym. Prepr.* **2000**, *41*, 1193–1194.
(39) Zong, X.; Kim, K.; Fang, D.; Ran, S.; Ran, S.; Hsiao, B. S.; Chu, B. *Polymer* **2002**, *43*, 4403–44120.
(40) Deitzel, J. M.; Kleinmeyer, J. D.; Hirvonen, J. K.; Tan, N. C. B. *Polymer* **2001**, *42*, 8163–8170.

and off in different regions of contact. Thinner fibers possess a higher degree of crystallinity, crystallite, and molecular orientation compared to thicker fibers, and these structural factors enhance the tendency of the "temporary dipoles" to orientate and increase the uneven charge distribution per unit area, resulting in higher adhesion strength.

Dry adhesion differs from wet adhesion in that it is mainly caused by the presence of vdW interaction without water meniscus (surface tension)[3] and hydrogen bonding. Since PCL is relatively hydrophobic, the adhesion tests are performed in an environment with relative humidity ~20%. As a result, the vdW is likely to contribute most significantly to the adhesion between electrospun fibers. The following analysis is provided for hypothetical consideration of vdW as the primary driving force behind adhesion of the studied fibers. The vdW energy of interaction U_{vdW} between two fibers is given by

$$U_{vdW} = 2\gamma = -A/12\pi D_{vdW} \quad (5)$$

where A is the materials-dependent Hamaker constant and D_{vdw} a vdW force range. Assuming $U_{vdW} = 190$ mJ/m^2 and $D_{vdW} = 0.3$ nm,[2] $A = 6.4 \times 10^{-19}$ J for PCL fibers, the order of magnitude of which is consistent with the values reported in the literature, $\sim 1.35 \times 10^{-19}$ J.[41] The slight variation can be caused by the testing conditions and environment, the type of monomers and molecular weights supplied, and the assumption of D_{vdW}, which can vary from material to another. Monolayers of water can also be present in our testing conditions of a relative humidity of ~20%. This hypothetical consideration corroborates that the vdW is the primary force behind the adhesion between two electrospun PCL fibers in this study. Note that the analysis is not definitive but supports the results that the adhesion measured is consistent with the vdW range.

(41) Isreakachvili, J. *Intermolecular and Surface Forces*; Academic: New York, 1992.

4. Conclusions

Do electropsun polymer fibers stick? In this study, we reported by direct measurement the adhesion strength and energy for two adhering electrospun fibers of PCL using a nanoforce tensile tester. The adhesion strength was found to fall in the range of 10^{-6} N and the adhesion energy 190 ± 7 mJ/m^2, which are nearly 4 times higher than that reported for PCL films. The adhesive strength increases with decreasing fiber radius, and the experimental data were described by the classical JKR model. On the basis of our analyses, the vdW were the primary driving force behind adhesion in electrospun micro- and nanofibers, while we did not rule out other environmental factors such as surface tension with hydro-monolayers. The molecular orientation and crystallinity of electrospun fibers were examined and suggested to play important roles in influencing adhesive properties. Why a higher fiber density is required to provide sufficient adhesion to support higher loads was analyzed and discussed. The study provided fruitful insights into applications of electrospun fibers for adhesion and the development of an electrospun nanofiber as a cheese cutter for small objects such as membranes and cytoplasm in future.

Acknowledgment. This work is primarily supported by the National Science Foundation under three CAREER Awards to S.-C.W. (NSF-CMMI 0746703), K.-T.W. (NSF-CMMI 0757140), and T.A.B. (NSF-IOS 0745379). Q.S. is partially supported by National Natural Science Foundation of China (Project No. 50803061, 50833005, and 50920105302). The authors thank the reviewers for their constructive comments on this manuscript.

Supporting Information Available: Video of "pull-off" process during adhesion measurement. This material is available free of charge via the Internet at http://pubs.acs.org.